

Polarimetry with NICMOS

Dean C. Hines¹, Glenn Schneider²

Abstract. NICMOS cameras 1 and 2 (with ~ 43 and ~ 76 mas/pixel, respectively) each carry a set of three polarizing elements to provide high sensitivity observations of linearly polarized light. The polarizers are bandpass limited and provide diffraction-limited imaging in camera 1 at 0.8 - 1.3 μ m, and in camera 2 at 1.9-2.1 μ m.

The NICMOS design specified the intra-camera primary axis angles of the polarizers to be differentially offset by 120°, and with identical polarizing efficiency and transmittance. While this ideal concept was not strictly achieved, accurate polarimetry in both cameras, over their full (11" and $\sim 19.2''$ square) fields of view was enabled through ground and on-orbit calibration of the as-built and *HST*-integrated systems.

The Cycle 7 & 7N calibration program enabled and demonstrated excellent imaging polarimetric performance with uncertainties in measured polarization fractions $\leq 1\%$. After the installation of the NICMOS Cooling System (NCS), the polarimetric calibration was re-established in Cycle 11, resulting in systemic performance comparable to (or better than) Cycle 7 & 7N.

The NCS era NICMOS performance inspired the development of an earlier conceived, but non-implemented, observing mode combining high contrast coronagraphic imaging and polarimetry in camera 2. This mode was functionally tested in the Cycle 7 GTO program, but without a detailed characterization of the instrumental polarization induced by the coronagraph, proper data calibration was not possible. To remedy this shortfall and to enable a new and powerful capability for NICMOS, we successfully executed a program to calibrate and commission the "Coronagraphic Polarimetry" mode in NICMOS in Cycle 13, and the mode was made available for GO use in Cycle 14.

We discuss the data reduction and calibration of direct and coronagraphic NICMOS polarimetry. Importantly, NICMOS coronagraphic polarimetry provides unique access to polarized light near bright targets over a range of spatial scales intermediate between direct polarimetry and ground-based (coronagraphic) polarimetry using adaptive optics.

1. Thermal Vacuum Tests

The NICMOS polarimetry systems were characterized on the ground during thermal vacuum tests using a light source that fully illuminated the field of view with completely linearly polarized light (i.e., $p(\%) = 100\%$) and with position angles variable in 5° increments. The polarizers in camera 1 and camera 2 are labeled by their nominal position angle orientation: POLS* for camera 1 and POLL* for camera 2. Camera 3 has three grisms that potentially act as polarizing elements, and were characterized as well. However, because the grisms

¹Space Science Institute, 4750 Walnut Street, Suite 205 Boulder, CO 80301

²Steward Observatory, The University of Arizona, 933 N. Cherry Ave., Tucson, AZ 85721

reside in the NIC3 filter wheel, they cannot be used with either the NIC1 or NIC2 polarizers and are unsuitable for spectropolarimetry.

The primary results of these thermal vacuum tests include:

- Each polarizer in each camera has a unique polarizing efficiency¹, with POL120S having the lowest at $\epsilon_{\text{POL120S}} = 48\%$.
- The angular offsets between the polarizers within each filter wheel differ from their nominal values of 120° .
- The instrumental polarization caused by reflections off the mirrors and optical baffles in the optical train is small ($\leq 1\%$).
- The gratings indeed act as partial linear polarizers, with the long wavelength grism (G206) producing the largest variation in intensity ($\sim 5\%$) for 100% linearly polarized light. If one measures the equivalent width of an emission line against a polarized continuum, the measurement will have different values depending on the orientation of the spacecraft *w.r.t.* the position angle of the polarized continuum. This effect scales with the source polarization, so should not be important for objects of low polarization ($p(\%) \leq 10\%$).

2. The Algorithm for Reducing NICMOS Polarimetry Observations

The thermal vacuum results showed that the standard reduction algorithm listed in basic optics text books would not work for NICMOS data. Instead, a more general approach was required (Hines, Schmidt & Lytle 1997; Hines 1998; Hines, Schmidt & Schneider 2000; Hines 2002).

At any pixel in an image, the observed signal from a polarized source of total intensity I and linear Stokes parameters Q and U measured through the k^{th} polarizer oriented at position angle φ_k is

$$S_k = A_k I + \epsilon_k (B_k Q + C_k U) . \quad (1)$$

Here,

$$A_k = \frac{t_k}{2}(1 + l_k), \quad B_k = A_k \cos 2\varphi_k, \quad C_k = A_k \sin 2\varphi_k , \quad (2)$$

ϵ_k is the polarizing efficiency, t_k is the fraction of light transmitted through the polarizer for a 100% linearly polarized input aligned with the polarizer axis, and l_k is the “leak” – the fraction of light transmitted through the polarizer (exclusive of that involved in t_k) when the incident beam is polarized perpendicular to the axis of the polarizer. These quantities are related under the above definitions, $\epsilon_k = (1 - l_k)/(1 + l_k)$.

This treatment can be shown to be equivalent to other approaches, once appropriate transformations are made (Mazzuca, Sparks, & Axon 1998; see also Sparks & Axon 1999).

The values of t_k were determined initially by the filter manufacturer from witness samples, and were not accurately remeasured during thermal vacuum tests. However, on-orbit observations of the unpolarized and polarized standard stars enables refinement of these numbers. Adopted characteristics of the individual polarizers and algorithm coefficients derived during and applicable to Cycle 7 & 7N are listed in Table 1 of Hines, Schmidt & Schneider (2000), the Cycle 11 coefficients are listed in Hines (2002), and are also available

¹Polarizing efficiency is defined as $\epsilon = (S_{\text{par}} - S_{\text{perp}})/(S_{\text{par}} + S_{\text{perp}})$, where S_{par} and S_{perp} are the respective measured signals for a polarizer oriented parallel and perpendicular to the position angle of a fully polarized beam.

in the NICMOS instrument manual and the *HST* Data Handbook. The primary coefficients are also listed in Table 1 in this contribution.

After solving the system of equations (eq. 1) for the Stokes parameters at each pixel (I, Q, U), the percentage polarization (p) and position angle (θ) are calculated in the standard way:

$$p = 100\% \times \frac{\sqrt{Q^2 + U^2}}{I}, \quad \theta = \frac{1}{2} \tan^{-1} \left(\frac{U}{Q} \right). \quad (3)$$

Note that a 360° arctangent function is assumed.

This algorithm has been tested by the NICMOS Instrument Definition Team (IDT) and by the Space Telescope Science Institute (STScI) on several data sets. An implementation has been developed by the IDT, and integrated into a software package written in IDL. The package is available through the STScI website² and is described by Mazzuca & Hines (1999). An update with improved graphical user interface will be available for Cycle 15.

3. The Cycles 7, 7N & 11 Polarimetry Characterization Programs

Observations of a polarized star (CHA-DC-F7: Whittet et al. 1992) and an unpolarized (null) standard (BD + 32 3739: Schmidt, Elston & Lupie 1992) were obtained with NIC1 and NIC2 in Cycle 7 & 7N (CAL 7692, 7958: Axon PI) and in Cycle 11 (CAL 9644: Hines PI). Data were obtained at two epochs such that the differential telescope roll between observations was $\approx 135^\circ$. This removes the degeneracy in position angle caused by the pseudo-vector nature of polarization. The second epoch observations in Cycle 7N and all of the observations in Cycle 11 used a four position, spiral-dither pattern with 20.5 pixel (NIC1) and 30.5 pixel (NIC2) offsets to improve sampling and alleviate the effects of bad pixels, some persistence, and other image artifacts. This is also the recommended observing strategy for all NICMOS, direct imaging polarimetry programs. While no dither pattern was used during the first epoch of Cycle 7, the data do not appear to suffer significantly from persistence. Observations of the highly polarized, proto-planetary nebula CRL 2688 (Egg Nebula) were also obtained to test the calibration over a large fraction of the field of view.

The observations were processed through the CALNICA pipeline at STScI using the currently available reference files. Aperture photometry was used to measure the total flux density from the stars in instrument units (DN/s) for each polarizer. The Stokes parameters were then constructed using equation (1). Since the thermal vacuum tests showed that the imaging optics themselves have little effect on the observed polarization, any measured polarization in the null standard was attributed the t_k term in the algorithm. The algorithm was applied to the polarized standard stars to check both the percentage polarization and the position angles.

The higher, yet more stable, operating temperature provided by the NCS and the three year dormancy of NICMOS may contribute to changes in the metrology of the optical system. Therefore, a program to re-characterize the polarimetry optics in Cycle 11 has been developed (NIC/CAL 9644: Hines).

The basic design of the Cycle 11 program follows the strategy undertaken in Cycle 7 & 7N, relying on observations of polarized and unpolarized standard stars as well as the proto-planetary nebula CRL 2688 (Egg Nebula). The Egg Nebula was only observed at a single epoch as a direct comparison with observations from Cycle 7 & 7N (ERO 7115: Hines; Sahai et al. 1998; Hines, Schmidt & Schneider 2000), and to evaluate any gross discrepancies across the field of view. Observations of the unpolarized standard star ($p(\%)_{\text{intrinsic}} = 0\%$, by definition) processed with the Cycle 7 & 7N algorithm coefficients yield $p_{\text{NIC1}} = 0.7\% \pm$

²http://www.stsci.edu/hst/nicmos/tools/polarize_tools.html

0.2%, $\theta_{\text{NIC1}} = 74^\circ$ and $p_{\text{NIC2}} = 0.7\% \pm 0.3\%$, $\theta_{\text{NIC2}} = 73^\circ$. This suggests that the system changed. The observations of the polarized standard star is also larger ($\Delta p \approx 2\%$) in NIC1 compared with the measurements of Cycle 7 & 7N, which themselves were in excellent agreement with ground-based measurements (Hines, Schmidt & Schneider 2000).

Observations of the Egg Nebula were also analyzed with the Cycle 7 & 7N coefficients. As for the polarized standard star, the results for the Egg Nebula suggest that the polarimetry system has changed slightly³, again by about 2% in p%.

We rederived the coefficients assuming that any measured polarization in the unpolarized (Q=U=0) standard was attributed to the t_k term in the algorithm (i.e. the variable term in the A_k coefficient). The new coefficients are listed in Table 1.

We note that we are embarking on a new study of all of the NICMOS direct imaging polarimetry calibration data in an attempt to improve the calibration to better than 0.3% (Batcheldor et al. 2006). This study was prompted by reports of a $\sim 1.5\%$ systematic residual polarization signal in some objects (e.g., Ueta et al. 2005). Indeed, Batcheldor et al. find a residual excess polarization for the ensemble of (un)polarized standard stars of $p(\%) \approx 1.2\%$, which behaves as a constant “instrumental” polarization that can be subtracted (in Stokes parameters) from the observations. While insignificant for highly polarized objects, this residual will affect observations of low polarization objects such as active galactic nuclei.

Due to the non-ideal polarimetry optical system, estimation of the uncertainties in the percentage polarization require a slightly more sophisticated analysis, especially for NIC 1. Monte Carlo simulations of the uncertainties based on the NICMOS performance are given in Hines, Schmidt & Schneider (2000), and an analytical approach is given in Sparks & Axon (1999). In particular, the usual assumption that $\sigma_q = \sigma_u$ is not valid for NIC 1.

4. Coronagraphic Polarimetry with NICMOS

Coronagraphic polarimetric observations of the same unpolarized and polarized standard stars that were used in Cycle 7, 7N (CAL 7692, 7958: Axon PI) and Cycle 11 (CAL 9644: Hines PI), and observations of the face-on circumstellar disk TW Hya were each obtained at two epochs sufficiently spaced in time to permit large differential rolls of the spacecraft (i.e., field orientations *w.r.t.* the HST optics and NICMOS polarizers). At each epoch, coronagraphic polarimetric imaging was carried out at two field orientations differing by 29.9° . Following standard NICMOS Mode-2 target acquisitions, the acquired targets were observed through each of the three “Long” wavelength polarizers in Camera 2. The intra-visit repeats for the standard stars were designed to check both for repeatability (image stability) and possible image persistence (none of consequence were found). TW Hya was exposed in only two repeats for each polarizer.

To facilitate commonality in data processing, all coronagraphic imaging was done with STEP16 multiaccum sampling, though the number of samples varied between 10 to 12 to best fill the orbits for each of the targets. The data were instrumentally calibrated in an APL-based analog to the STSDAS CALNICA task using on-orbit derived calibration reference files suitable for these observations. Following the creation of count rate images, individual bad pixels were replaced by 2D weighted Gaussian interpolation ($r=5$ weighing radius) of good neighbors, and “horizontal striping” associated with heavily exposed targets was characterized and removed by median-collapse subtraction.

³The polarization structure of the Egg is not expected to change over the 5 year period between observations even though the object is known to show photometric variations.

4.1. PSF-subtracted Images

The image data for this program were obtained to investigate and demonstrate the further suppression of instrumentally scattered light via the camera 2 coronagraph (compared to non-coronagraphic polarimetry) and thus effect a reduction in the detection floor for a polarized signal in the diffuse wings of the (suppressed) scattering component of the occulted PSF core. For this purpose, the data obtained were not optimized to enable coronagraphic PSF subtraction (see, e.g., Fraquelli et al. 2004). Imaging coronagraphy under the pass band Camera 2 1.9-1.2 μ m polarizers will be less effective than under the 1.4-1.8 μ m F160W (H band) filter. Imaging coronagraphy of our calibration science target, the very-near face-on TW Hya circumstellar disk under the F160W filter was discussed in Weinberger et al. (2002). The smaller inner working angle of the coronagraph with polarizers (caused by the longer wavelength pass-band), while fully enclosing the PSF core under the polarizers, permits light from the first Airy ring to escape the coronagraphic image plane mask.

Both the unpolarized standard BD +32 -3739 and the polarized standard CHA-DC-F7 were selected to establish “truth” *w.r.t.* the instrumental polarization (and ultimately sensitivity) with polarimetric coronagraphy. They were not chosen to serve as coronagraphic reference PSF’s for subtraction from TW Hya, and both calibration stars are significantly fainter than TW Hya. Additionally, the field of the unpolarized standard has a significant number of fainter stars near the target, unknown prior to the coronagraphic imaging resulting from this program. This is not a problem for the coronagraphic polarimetric calibration/validation, but as such that additionally makes it a poor choice as a PSF subtraction template star.

Nonetheless, DIRECT imaging of circumstellar dust from the Camera 2 polarizer set derived total intensity images is demonstrated (but not comprehensively in this summary) using this “template” PSF. The depth of exposure of BD+32 is insufficient to reveal the outer part of the TW Hya disk. The flux density rescaling of BD+32 is suggested as 3.48 from the 2MASS H and K magnitudes and the passband of the Camera 2 polarizers. The disk persists varying the BD+32 intensity over the full range of TW Hya:BD+32 intensities suggested in H and K, though very significant under- and over-subtraction residuals appear at the extreme of that range in the diffraction spikes, suggesting the a priori ratio was very close to “correct”.

4.2. Polarimetry Comparison Between the Unpolarized Star and TW Hya

After reduction of the images in the three different polarizers, the images were processed through the NICMOS polarimetry reduction algorithm (Hines, Schmidt & Schneider 2000) to produce images of the polarization position angle (θ), the percentage polarization, and the polarized intensity ($= p \times I$). To consider the detection of polarized flux to be “well determined” we demand the polarized intensity in any pixel be at least 5-sigma above the median of the background. For this data set we choose a background region far from the target, and away from the diffraction spikes, where no contribution to the background from the target flux is seen. With this, the centrosymmetric polarization field for the near-face on TW Hya disk is obvious, and highly repeatable, in all four field orientations of the TW Hya observations.

While some residual instrumental polarization seems apparent, the lack of obvious structure in the position angle image of the unpolarized standard star is dramatically different than that of the TW Hya position angle image; the TW Hya image shows the classic “butterfly” pattern for centrosymmetric polarization caused by scattering off a face-on disk. Furthermore, the median polarization is about 2% per resolution element for the “unpolarized” star, compared with $\sim 10 - 15\%$ per resolution element for TW Hya. The results for TW Hya are shown in Figure 1. The measured polarization in the disk is consistent with measurements made from the ground with Adaptive Optical systems (D. Potter, private comm., and Hales et al. 2005).

4.3. Continued Analysis

Our analysis so far has shown that the mode is viable for future Cycles. We have sufficient data in hand to evaluate:

- The ability to remove the small instrumental polarization signature in Stokes parameter space.
- The spatial correlation of this instrumental polarization as a function of radius and azimuth with respect to the coronagraphic hole.
- The polarization sensitivity as a function of radius from the coronagraphic hole. This analysis is limited by the exposure depth of the unpolarized standard.

4.4. Recommendations

Based upon our preliminary analysis, we recommend that NICMOS coronagraphic polarimetry be released as an available mode for future Cycles. We note that the same rules that apply to direct coronagraphic imaging apply to this mode as well. In particular, the fine guidance necessary to keep the target well centered in the hole is necessary. In addition, we recommend that observations be obtained at two-roll angles to interpolate over bad pixels and develop an in situ flat field correction near the coronagraphic hole. This may be difficult to achieve in two-gyro mode.

We cannot yet tell if the current calibration data from Cycle 12 will be sufficient for GOs. At present, we would urge that GOs observe their target plus an unpolarized standard star, each at sufficient depth to obtain similar S/N in each object in each polarizer thus a minimum of two orbits for a single target program. However, a single, well exposed unpolarized standard star should be sufficient for a multi-target science program.

5. Two-Gyro Mode

Based upon the measured jitter in two-gyro mode, there should be no degradation of the direct polarimetry mode. Tests of coronagraphic imaging also suggest minimal degradation (Schneider et al. 2005, ISR2005-001). The primary impact will be the inability to obtain images at two spacecraft roll angles within a single orbit.

6. Summary

A wide variety of astronomical objects have been examined with NICMOS direct imaging polarimetry including Active Galaxies (Capetti et al. 2000; Tadhunter et al. 2000; Simpson et al. 2002), evolved stars and proto-planetary nebulae (Sahai et al. 1998; Weintraub et al. 2000; Schmidt, Hines & Swift 2002; King et al. 2002; Su et al. 2003; Ueta et al. 2005), and young stellar objects (Silber et al. 2000; Meakin, Hines & Thompson 2005). NICMOS continues to provide high fidelity, high spatial resolution imaging polarimetry. Combined with the polarimetry mode of the Advanced Camera for Surveys (ACS), *HST* provides high resolution imaging polarimetry from $\sim 0.2 - 2.1\mu\text{m}$. With the newly commissioned coronagraphic polarimetry mode, NICMOS provides further unique access to polarized light near bright targets over a range of spatial scales intermediate between direct polarimetry and ground-based (coronagraphic) polarimetry using adaptive optics.

An electronic version of the presentation given by D.C. Hines at the workshop can be found at the following URL:

<http://www.stsci.edu/ts/webcasting/ppt/CalWorkshop2005/DeanHines102805.ppt>

References

- Capetti, A., et al. 2000, ApJ, 544, 269
- Fraquelli, D. A., Schultz, A. B., Bushouse, H., Hart, H. M., & Vener, P. 2004, PASP, 116, 55
- Hales, A. S., Gledhill, T. M., Barlow, M. J., & Lowe, K. T. E. 2005, ArXiv Astrophysics e-prints, arXiv:astro-ph/0511793
- Hines, D. C., 2003, in *Proc. 2002 HST Calibration Workshop*, ed. S. Arribas, A. Koekemoer, & B. Whitmore (Baltimore: STScI), p. 260
- Hines, D.C., Schmdit, G.D. & Schneider, G. 2000, PASP, 112, 983
- Hines, D. C. 1998, NICMOS and the VLT: A New Era of High Resolution Near Infrared Imaging and Spectroscopy, Pula, Sardinia, Italy, June 26-27th 1998 ESO Conference and Workshop Proceedings 55, 1998, Wolfram Freudling and Richard Hook eds., p. 63, 63
- Hines, D. C., Schmidt, G. D., & Lytle, D. 1997, *The 1997 HST Calibration Workshop with a New Generation of Instruments*, p. 217, 217
- King, N. L., Nota, A., Walsh, J. R., Panagia, N., Gull, T. R., Pasquali, A., Clampin, M., & Bergeron, L. E. 2002, ApJ, 581, 285
- Mazzuca, L., Sparks, B., & Axon, D. 1998, *Instrument Science Report NICMOS 98-017* (Baltimore: STScI), available through <http://www.stsci.edu/hst/nicmos>
- Mazzuca, L. & Hines, D.C. 1999, *Instrument Science Report NICMOS 99-004* (Baltimore: STScI)
- Meakin, C. A., Hines, D. C., & Thompson, R. I. 2005, ApJ, 634, 1146
- Sahai, R., Hines, D. C., Kastner, J. H., Weintraub, D. A., Trauger, J. T., Rieke, M. J., Thompson, R. I., & Schneider, G. 1998, ApJ, 492, L163
- Schmidt, G. D., Elston, R., & Lupie, O. L. 1992, AJ, 104, 1563
- Schmidt, G. D., Hines, D. C., & Swift, S. 2002, ApJ, 576, 429
- Silber, J., Gledhill, T., Duchêne, G., & Ménard, F. 2000, ApJ, 536, L89
- Simpson, J. P., Colgan, S. W. J., Erickson, E. F., Hines, D. C., Schultz, A. S. B., & Trammell, S. R. 2002, ApJ, 574, 95
- Sparks, W.B., & Axon, D.J. 1999, PASP, 111, 1298
- Su, K. Y. L., Hrivnak, B. J., Kwok, S., & Sahai, R. 2003, AJ, 126, 848
- Ueta, T., Murakawa, K., & Meixner, M. 2005, AJ, 129, 1625
- Tadhunter, C. N., et al. 2000, MNRAS, 313, L52
- Thompson, R. I., Rieke, M., Schneider, G., Hines, D. C., & Corbin, M. R. 1998, ApJ, 492, L95
- Weinberger, A. J., Becklin, E. E., Schneider, G., Chaing, E. I., Lowrance, P. J., Silverstone, M., Zuckerman, B., Hines, D. C. & Smith, B. A., 2002, ApJ, 566, 409
- Weintraub, D. A., Kastner, J. H., Hines, D. C., & Sahai, R. 2000, ApJ, 531, 401

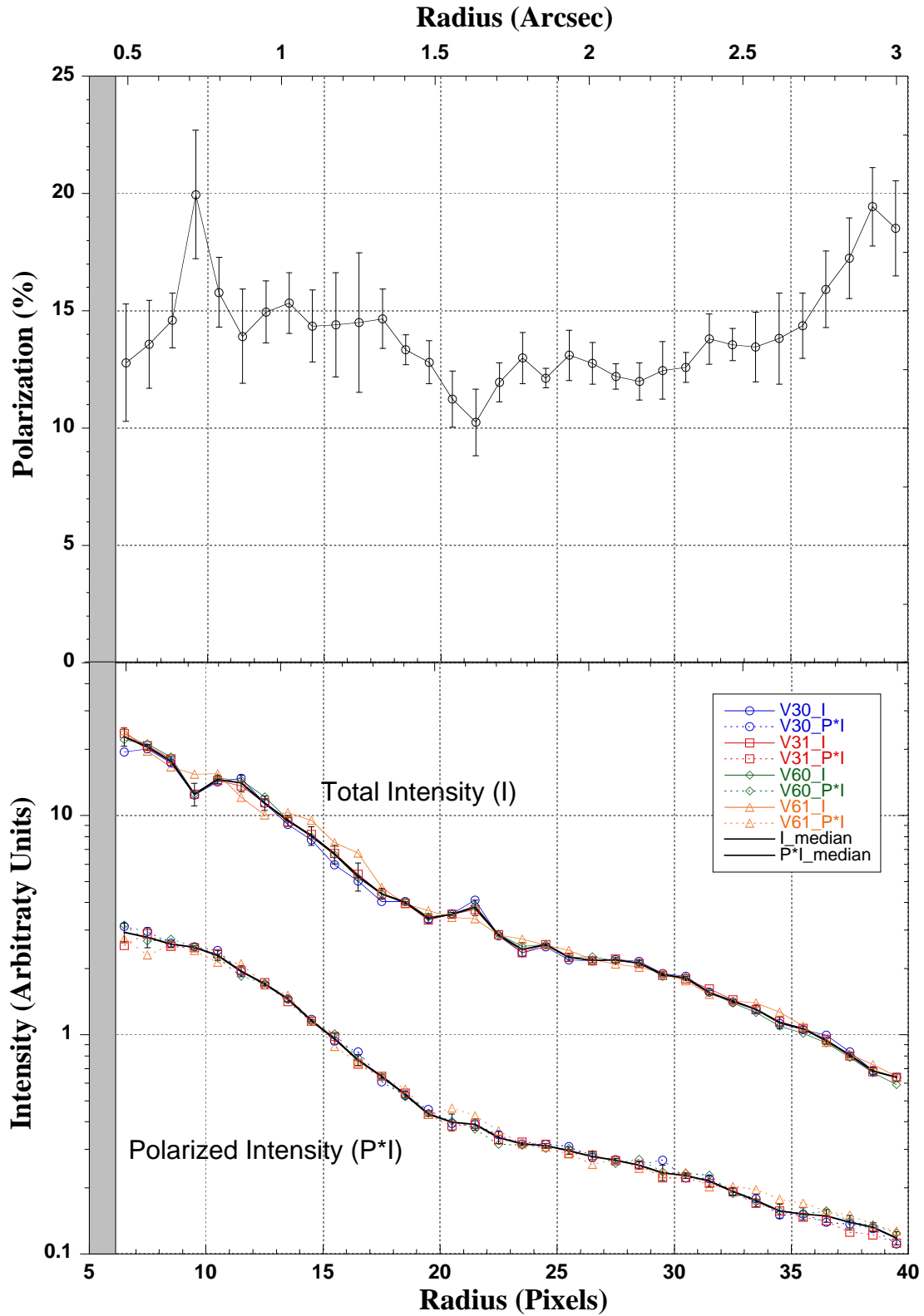


Figure 1: Coronagraphic polarimetry of TW Hya. The top panel shows the percentage polarization. The bottom panel shows the azimuthally averaged total intensity and the polarized intensity.

Table 1. Characteristics of the NICMOS Polarizers & Coefficients to Eq. (1)

Filter	φ_k	ϵ_k	$t_k(\text{Pre-NCS})^a$	$t_k(\text{NCS})^a$	Comments
POL0S	1.42	0.9717	0.7760	0.7760	Ghosts
POL120S	116.30	0.4771	0.5946	0.5934	Weak ghosts
POL240S	258.72	0.7682	0.7169	0.7173	Ghosts
POL0L	8.84	0.7313	0.8981	0.8779	...
POL120L	131.42	0.6288	0.8551	0.8379	...
POL240L	248.18	0.8738	0.9667	0.9667	...

^aDerived from on-orbit observations of the unpolarized standard star BD+32°3739 (Schmidt, Elston & Lupie 1992).